PTEP

Prog. Theor. Exp. Phys. **2016**, 031E02 (8 pages)
DOI: 10.1093/ptep/ptw015

Letter

The detection of quasinormal mode with $a/M = 0.95$ would prove a sphere 99% soaking in the ergoregion of the Kerr space-time[1]

Hiroyuki Nakano*, Takashi Nakamura, and Takahiro Tanaka

Department of Physics, Kyoto University, Kyoto 606-8502, Japan
*E-mail: hinakano@yukawa.kyoto-u.ac.jp

Received January 19, 2016; Revised February 5, 2016; Accepted February 5, 2016; Published March 24, 2016

Recent numerical relativity simulations of mergers of binary black holes suggest that the maximum final value of a/M is $\sim$0.95 for the coalescence of two equal-mass black holes with aligned spins of the same magnitude $a/M = 0.994$, which is close to the upper limit $a/M = 0.998$ of accretion spin-up shown by Thorne [Astrophys. J. **191**, 507 (1974)]. Using the Wentzel–Kramers–Brillouin method, we suggest that, if quasinormal modes with $a/M \sim 0.95$ are detected by second-generation gravitational wave detectors, we could confirm the strong gravity space-time based on Einstein's general relativity up to $1.33M$, which is only $\sim$1.014 times the event horizon radius and within the ergoregion. One more message about black hole geometry is expected here. If the quasinormal mode is different from that of general relativity, we need to find the true theory of gravity that deviates from general relativity only near the black hole horizon.

Subject Index E01, E02, E31, E38

1. *Introduction* The Kerr space-time [1], which describes a rotating black hole (BH), is very interesting not only in astrophysics but also in mathematics and physics. In particular, the existence of the ergoregion induces various phenomena specific to strongly curved space-time, such as the Penrose process [2], by which we can extract the rotational energy of the BH.

To confirm the space-time described by the Kerr BH using second-generation gravitational wave detectors such as Advanced LIGO (aLIGO) [3], Advanced Virgo (AdV) [4], and KAGRA [5,6], we discuss gravitational waves of the quasinormal modes (QNMs), which are the unique signature of the gravitational wave emission from a BH. We expect that the gravitational waves are emitted when a BH is formed after the merger of compact objects, and, e.g., the possible detection rate of BH–BH mergers was discussed in our previous paper [7].

It would be interesting here to observe that there may be an astrophysical restriction on the spin of BHs. From the mass formula of a BH [8], we have the gravitational mass of M as

$$M^2 = \frac{2M_{\rm irr}^2}{1+\sqrt{1-q^2}}, \tag{1}$$

where $q = a/M$ with the BH's specific angular momentum a, and $M_{\rm irr}$ is the irreducible mass of the Kerr BH, which is related to the area of the event horizon A as $A = 16\pi M_{\rm irr}^2$. For a single BH,

[1] This letter is dedicated to the memory of Professor Steven Detweiler.

Thorne [9] showed that the maximum value of $q_{\rm max}$ is $\sim$0.998 since the radiation emitted by the accretion disk carries the angular momentum to prevent the BH from reaching the extremal limit, $q = 1$. Now, let us consider the merger of two equal-mass Kerr BHs of mass M with the maximum value of aligned spins $q = q_{\rm max}$, which results in a single BH with the final mass M_f and $q = q_f$. Since the area of the horizon should increase [10] (see also Ref. [11]), we have

$$1 + \sqrt{1 - q_f^2} \geq \frac{2M^2}{M_f^2}\left(1 + \sqrt{1 - q_{\rm max}^2}\right) = \frac{2.126M^2}{M_f^2}. \tag{2}$$

This means that, if $M_f \geq 1.46M$, $q_f = 1$ is possible, in contrast to the accretion spin-up model by Thorne [9]. However, even in a recent numerical relativity simulation of a binary BH merger with equal mass $M_1 = M_2 = M$ and aligned equal spins with $q_1 = q_2 = 0.994$ by Scheel et al. [12], q_f is $\sim$0.95. Therefore, we restrict our study up to $q_f = 0.97$ here.

In our previous paper [7], we presented a method to claim how close to the event horizon of a BH we actually *see* by gravitational wave detection of the QNMs. In that paper, our focus was not on determining the QNM frequencies accurately at all. Instead, we used the known accurate numerical results of the complex QNM frequencies and the separation constant λ in the Teukolsky equation [13] to suggest which part of strong gravity space-time is confirmed by the detection of QNMs. In the present letter, using the same approach, we discuss further whether we can reach the confirmation of the space-time region within the ergoregion by the QNM gravitational wave detection.

This letter is organized as follows. In Sect. 2, we will argue our method briefly. The results are given in Sect. 3 and Sect. 4 is devoted to discussions. We use the geometric unit system, where $G = c = 1$, in this letter.

2. *Approach*

In the Boyer–Lindquist coordinates, the Kerr metric is given by

$$ds^2 = -\left(1 - \frac{2Mr}{\Sigma}\right)dt^2 - \frac{4Mar\sin^2\theta}{\Sigma}dt\,d\phi + \frac{\Sigma}{\Delta}dr^2 + \Sigma d\theta^2 + \left(r^2 + a^2 + \frac{2Ma^2r}{\Sigma}\sin^2\theta\right)\sin^2\theta d\phi^2, \tag{3}$$

where M and a are the mass and the spin parameter, respectively, $\Sigma = r^2 + a^2\cos^2\theta$, and $\Delta = r^2 - 2Mr + a^2$. We summarize here three characteristic radii in this Kerr space-time. The event horizon is located at

$$r_+ = M\left(1 + \sqrt{1 - q^2}\right), \tag{4}$$

and the inner light ring radius [14] is at

$$r_{\rm lr} = 2M\left\{1 + \cos\left[\tfrac{2}{3}\cos^{-1}(-q)\right]\right\}, \tag{5}$$

which is evaluated in the equatorial ($\theta = \pi/2$) plane. In Ref. [15] (and references therein), the relation between this light ring orbit and the QNM frequencies in the high-frequency regime was discussed. Also, the ergosurface is given by

$$r_{\rm ergo}(\theta) = M\left(1 + \sqrt{1 - q^2\cos^2\theta}\right), \tag{6}$$

and we denote the equatorial radius of the ergoregion as

$$r_{\rm ergo} = 2M. \tag{7}$$

In the previous paper [7], we extended the physical picture of QNMs by Schutz and Will [16] for the Schwarzschild space-time via the Wentzel–Kramers–Brillouin (WKB) method to the Kerr

space-time. Given the radial wave equation,

$$\frac{d^2X}{dr^{*2}} + \left(\omega^2 - V_{\rm D}\right) X = 0, \tag{8}$$

where $dr^*/dr = \left(r^2 + a^2\right)/\Delta$ and $V_{\rm D}$ is a potential that is obtained from the potential of the Teukolsky radial equation [13]. Here, we approximate the potential by the expansion near the radius at its peak location r_0^* as

$$V_{\rm D}(r^*) = V_{\rm D}(r_0^*) + \frac{1}{2}\left.\frac{d^2V_{\rm D}}{dr^{*2}}\right|_{r^*=r_0^*}(r^* - r_0^*)^2. \tag{9}$$

Here, r_0^* is related to the peak location in the Boyer–Lindquist radial coordinate as

$$r_0^* = r_0 + \frac{2}{r_+ - r_-}\left[r_+ \ln\left(\frac{r_0 - r_+}{2}\right) - r_- \ln\left(\frac{r_0 - r_-}{2}\right)\right], \tag{10}$$

where $r_- = M\left(1 - \sqrt{1 - q^2}\right)$. In practice, we determine r_0^* by evaluating the peak location of the absolute value of the potential in Eq. (8). In the appendix of Ref. [7], we also discussed the location of r^* that satisfies $dV/dr^* = 0$ in the complex radius plane, and then read off the effective peak radius from the real part of the complex radius, to find no significant difference between the two radii.

Then, the QNM frequencies are derived as

$$\omega^2 = \left(\omega_r + i\omega_i\right)^2 = V_{\rm D}(r_0^*) - i\sqrt{-\frac{1}{2}\left.\frac{d^2V_{\rm D}}{dr^{*2}}\right|_{r^*=r_0^*}}, \tag{11}$$

in the leading-order WKB analysis.

In Ref. [7], we used the WKB approximation to determine QNMs by using the spatial positions of the maximum absolute values of the Sasaki–Nakamura potential $V_{\rm SN}$ [17–19] and the Detweiler potential $V_{\rm D}$ [20] up to $q = 0.8$ since the remnant spin $q_f \sim 0.7$ is expected from the results of numerical relativity for the merger of equal-mass BHs with $q_1 = q_2 = 0$ [21–23]. In this letter, we consider up to $q_f = 0.97$ since a recent result of numerical relativity for $q_1 = q_2 \sim q_{\rm max}$ [12] yields $q_f \sim 0.95$.

Also, in this letter, we treat the Detweiler potential [20] (the $(-+)$ case in Ref. [7]) as the potential $V_{\rm D}$. This is because the $(-+)$ potential has a less wavy shape and looks most suitable compared with the other cases for the WKB analysis (see Figs. 1 and 5 of Ref. [7]). We do not repeat how to derive $V_{\rm D}$ since the details are given in Sect. 4 of Ref. [7].

In the following, we focus only on the $(\ell = 2,\ m = 2)$ mode. This is because the $(\ell = 2,\ m = 2)$ QNM is dominant in numerical relativity simulations of binary BH mergers (see, e.g., Ref. [24]) even in the case of the remnant spin $q_f \sim 0.95$ [12] (we can check the behavior by using the waveforms in the SXS Gravitational Waveform Database [25]).

3. *Results* First, we present the behavior of the real part of the potential $\mathrm{Re}(V_{\rm D})$, the imaginary part $\mathrm{Im}(V_{\rm D})$, and the absolute value $|V_{\rm D}|$ for various nondimensional spin parameters in Figs. 1 and 2. The three panels in Fig. 1 are for $q = 0.7$ (left), 0.8 (center), and 0.9 (right). We find that the contribution of the imaginary part is small even for $q = 0.9$. On the other hand, the three panels in Fig. 2 shows the potential for $q = 0.93$ (left), 0.95 (center), and 0.97 (right). Again, the contribution of the imaginary part is small, but we see another peak around $r^*/M \sim 5$ in the $q = 0.97$ case (in practice, we also see another peak in the $q = 0.95$ case outside the figure). This peak grows for

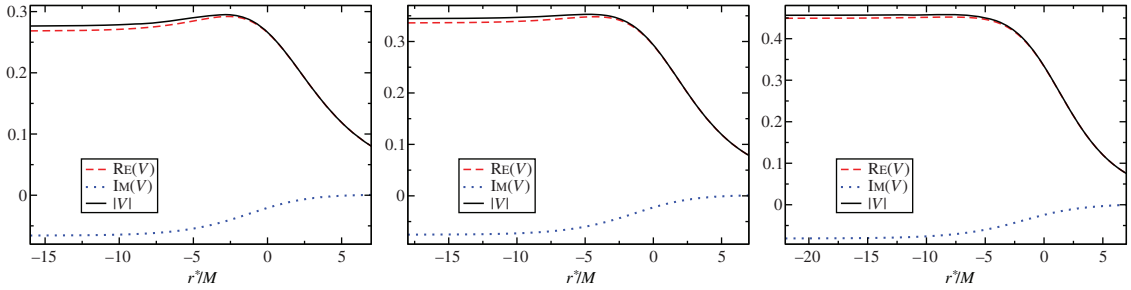

Fig. 1. $\mathrm{Re}(V_{\mathrm{D}})$, $\mathrm{Im}(V_{\mathrm{D}})$, and $|V_{\mathrm{D}}|$ with $(\ell = 2,\ m = 2)$ for $q = 0.7$ (left), 0.8 (center), and 0.9 (right) with each QNM frequency as a function of r^*/M where we set $M = 1$. The contribution of the imaginary part is small.

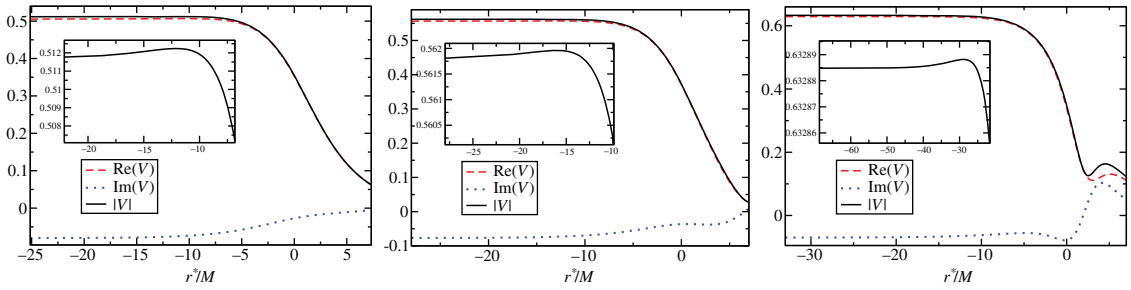

Fig. 2. $\mathrm{Re}(V_{\mathrm{D}})$, $\mathrm{Im}(V_{\mathrm{D}})$, and $|V_{\mathrm{D}}|$ with $(\ell = 2,\ m = 2)$ for $q = 0.93$ (left), 0.95 (center), and 0.97 (right) with each QNM frequency as a function of r^*/M where we set $M = 1$. The contribution of the imaginary part is still small. The inset of each panel shows the existence of the maximum of $|V_{\mathrm{D}}|$.

Table 1. The event horizon radius, the peak location of the absolute value of the potential V_{D}, and the location of r that satisfies $dV_{\mathrm{D}}/dr^* = 0$ in the complex radius plane. We also show the WKB result of $\mathrm{Im}(\omega)M$. The solid angle of a sphere of r_{peak} soaking in the ergoregion $(4\pi C)$ is estimated by Eq. (12).

q	r_+/M	r_{peak}/M	$r_{dV_{\mathrm{D}}/dr^*=0}/M$	WKB $\mathrm{Im}(\omega)M$	C
0.7	1.7141	1.9699	$1.9941 + 0.155\,60i$	−0.082 273	0.347 86
0.8	1.6	1.7585	$1.7852 + 0.156\,97i$	−0.076 730	0.814 59
0.9	1.4359	1.4969	$1.5169 + 0.130\,98i$	−0.066 175	0.964 23
0.91	1.4146	1.4664	$1.4850 + 0.125\,42i$	−0.064 379	0.972 06
0.92	1.3919	1.4348	$1.4517 + 0.119\,06i$	−0.062 330	0.978 83
0.93	1.3676	1.4018	$1.4171 + 0.111\,81i$	−0.059 964	0.984 65
0.94	1.3412	1.3670	$1.3808 + 0.103\,56i$	−0.057 193	0.989 60
0.95	1.3122	1.3301	$1.3425 + 0.094\,182i$	−0.053 913	0.993 63
0.96	1.28	1.2901	$1.3018 + 0.083\,455i$	−0.049 916	0.996 87
0.97	1.2431	1.2454	$1.2583 + 0.070\,499i$	−0.044 759	0.999 40

larger q and the height of the peak becomes dominant in the $q = 0.98$ case. Therefore, we restrict our analysis up to $q = 0.97$, which is appropriate since the recent numerical relativity results suggest $q_f \lesssim 0.95$ [12].

In Table 1, we summarize the event horizon radius r_+, the peak location (r_{peak}) of the absolute value of the potential V_{D}, and the location that satisfies $dV_{\mathrm{D}}/dr^* = 0$ in the complex radius plane, $r_{dV_{\mathrm{D}}/dr^*=0}$. The differences between the real part of $r_{dV_{\mathrm{D}}/dr^*=0}$ and r_{peak} are small, and the imaginary part of $dV_{\mathrm{D}}/dr^* = 0$ is also small. In the same table, we also show the WKB result of $\mathrm{Im}(\omega)M$ and

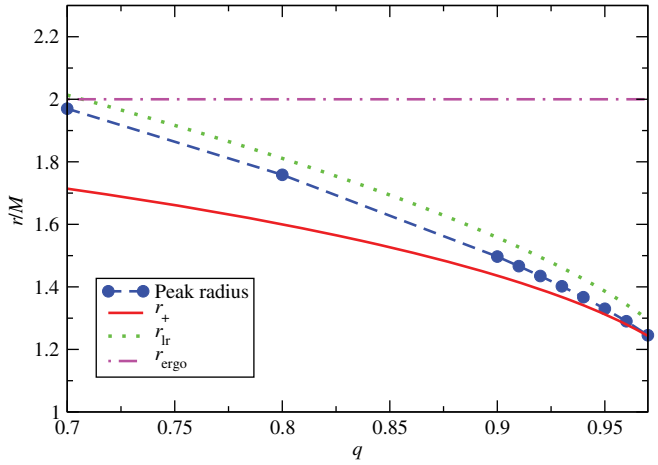

Fig. 3. The location of the maximum of the absolute value of the potential $|V_{\rm D}|$ with $(\ell = 2, m = 2)$. We also show the event horizon $r_+/M = 1 + \sqrt{1-q^2}$, the inner light ring radius $r_{\rm lr}/M = 2(1 + \cos((2/3)\cos^{-1}(-q)))$, and the equatorial radius of the ergoregion $r_{\rm ergo}/M = 2$ evaluated for various spin parameters $q = a/M$.

the solid angle of a sphere of $r_{\rm peak}$ soaking in the ergoregion $(4\pi C)$ estimated as

$$C = \frac{1}{2}\int_{\theta_{\rm m}}^{\pi-\theta_{\rm m}} \sin\theta d\theta, \tag{12}$$

where $\theta_{\rm m}$ is calculated by $r_{\rm peak} = M\left(1 + \sqrt{1 - q^2\cos^2\theta_{\rm m}}\right)$. The timelike Killing vector field of the Kerr space-time becomes spacelike in the ergoregion, and the region is coordinate invariant. Here, we have introduced this C as an estimator that is less dependent on the coordinates, while the radial coordinate is variant.

The peak location ($r_{\rm peak}$) of the absolute value of the potential $V_{\rm D}$ in Table 1 is plotted in Fig. 3. In this figure, we also show the event horizon radius r_+, the inner light ring radius $r_{\rm lr}$, and the equatorial radius of the ergoregion $r_{\rm ergo}$.

The real and imaginary parts of the $n = 0$ QNM frequencies are shown in the left panel of Fig. 4, respectively. Here, we present the WKB result and the exact frequencies given in Ref. [26]. We find that the errors are quite small in this spin range (see the right panel of Fig. 4).

4. *Discussions* In our previous paper [7], we assumed a remnant BH spin of $q_f = 0.7$ to compute the detection rate. When we treat BHs with $q_f = 0.95$, two effects from the QNM frequency arise; i.e., the (real part of the) frequency of the QNM increases while the damping rate decreases. Therefore, a recalculation is needed (note that the QNM amplitude (excitation) is also an important input). However, the former effect will decrease the event rate while the latter effect increases the event rate. Therefore, the event rate will be more or less similar. This means that the merging rate of Pop III $\sim 30M_\odot$–$30M_\odot$ BH binaries with the signal-to-noise ratio >35 needed for the determination of QNMs [28] is roughly 0.17–7.2 events yr^{-1} $({\rm SFR_p}/(10^{-2.5}\ {\rm M_\odot\ yr^{-1}\ Mpc^{-3}}))\cdot([{\rm f_b}/(1+{\rm f_b})]/0.33)$ where $\rm SFR_p$ and $\rm f_b$ are the peak value of the Pop III star formation rate and the fraction of binaries, respectively [29,30].

As seen in Fig. 3, the location of the maximum of the absolute value of the potential is within the ergoregion for $q \gtrsim 0.7$. It is noted that in Table 1 the spin, the imaginary part of the QNM frequency,

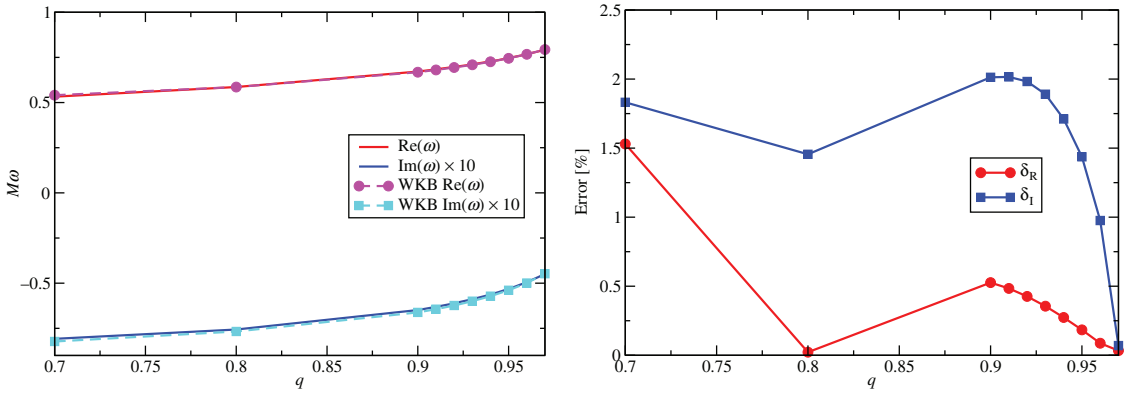

Fig. 4. (Left) The real and imaginary parts of the fundamental ($n = 0$) QNM frequencies with $V_{\rm D}(\ell = 2,\ m = 2)$ evaluated for various spin parameters $q = a/M$. The exact frequencies Re(ω) and Im(ω) are from Refs. [26,27]. (Right) Absolute value of relative errors for the real and imaginary parts of the QNM frequencies with $V_{\rm D}(\ell = 2,\ m = 2)$, $\delta_{\rm R} = |(\text{WKB Re}(\omega))/\text{Re}(\omega) - 1|$, and $\delta_{\rm I} = |(\text{WKB Im}(\omega))/\text{Im}(\omega) - 1|$ between the exact value and that of the WKB approximation.

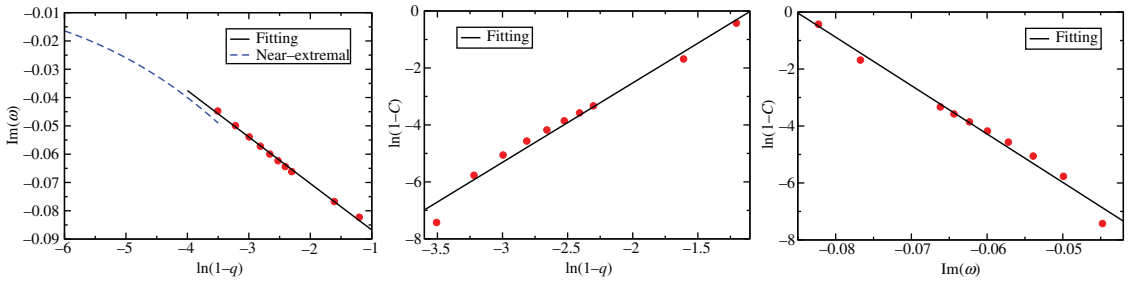

Fig. 5. The red points are from Table 1, and the black lines show Eqs. (13) obtained by linear fitting. In the left panel, we also present Eq. (14) by the blue dashed curve.

and the solid angle of a sphere of $r_{\rm peak}$ soaking in the ergoregion have simple relations,

$$\begin{aligned} M\text{Im}(\omega) &= -0.016\,416\,\ln(1-q) - 0.1032, \\ \ln(1-C) &= 2.7867\,\ln(1-q) + 3.0479, \\ \ln(1-C) &= -169.92\,M\text{Im}(\omega) - 14.476, \end{aligned} \tag{13}$$

in the range between $q = 0.7$ and 0.97 (see Fig. 5). Related to the existence of the event horizon, it is important to know how far we can confirm the ergoregion by gravitational wave detection of the QNMs. The above relations give us the direct relation between C and the imaginary part of the observed QNM frequency.

Here, according to Hod [31], the imaginary part of the QNM frequency for near-extremal Kerr BHs is

$$M\text{Im}(\omega) = -\frac{\sqrt{1-q^2}}{4\left(1+\sqrt{1-q^2}\right)}, \tag{14}$$

which is shown as the blue dashed curve in the left panel of Fig. 5. The difference between Eqs. (13) and (14) can be considered as the next-order effect of the near-extremal approximation. We will clarify the physical meaning of Eqs. (13) in future work.

Finally, it is necessary to investigate QNMs in the case of $q > 0.97$, which requires some high-accuracy study (see, e.g., Ref. [32]). Also, there are many excited states [33] that contribute to the QNM gravitational waves. A detailed study is needed for a fully integrated understanding of QNMs.

In conclusion, we have covered the QNM analysis of the Kerr BH up to $q \sim 0.95$ in this letter. This spin parameter $q \sim 0.95$ is expected by state-of-the-art numerical relativity simulations of mergers of an equal-mass, highly spinning BH binary with aligned spins of the same magnitude $q = 0.994$. The detection of the QNM with $a/M \sim 0.95$ by second-generation gravitational wave detectors would prove a sphere 99% soaking in the ergoregion of the Kerr BH, and such a space-time region will give us the opportunity to test Einstein's general relativity in strong gravity.

Acknowledgements

This work was supported by a MEXT Grant-in-Aid for Scientific Research on Innovative Areas, "New Developments in Astrophysics Through Multi-Messenger Observations of Gravitational Wave Sources", No. 24103006 (H.N., T.N., T.T.) and by a Grant-in-Aid from the Ministry of Education, Culture, Sports, Science and Technology (MEXT) of Japan, No. 15H02087 (T.N., T.T.).

References

[1] R. P. Kerr, Phys. Rev. Lett. **11**, 237 (1963).
[2] R. Penrose, Riv. Nuovo Cimento **1**, 252 (1969) [Gen. Relat. Gravit. **34**, 1141 (2002)].
[3] J. Aasi et al. [LIGO Scientific Collaboration], Class. Quantum Grav. **32**, 074001 (2015) [arXiv:1411.4547 [gr-qc]] [Search INSPIRE].
[4] F. Acernese et al. [VIRGO Collaboration], Class. Quantum Grav. **32**, 024001 (2015) [arXiv:1408.3978 [gr-qc]] [Search INSPIRE].
[5] K. Somiya, [KAGRA Collaboration], Class. Quantum Grav. **29**, 124007 (2012) [arXiv:1111.7185 [gr-qc]] [Search INSPIRE].
[6] Y. Aso et al. [KAGRA Collaboration], Phys. Rev. D **88**, 043007 (2013) [arXiv:1306.6747 [gr-qc]] [Search INSPIRE].
[7] T. Nakamura, H. Nakano, and T. Tanaka, [arXiv:1601.00356 [astro-ph.HE]] [Search INSPIRE].
[8] C. W. Misner, K. S. Thorne, and J. A. Wheeler, *Gravitation* (Freeman, San Francisco, CA, 1973).
[9] K. S. Thorne, Astrophys. J. **191**, 507 (1974).
[10] S. W. Hawking, Commun. Math. Phys. **25**, 152 (1972).
[11] J. M. Bardeen, B. Carter, and S. W. Hawking, Commun. Math. Phys. **31**, 161 (1973).
[12] M. A. Scheel, M. Giesler, D. A. Hemberger, G. Lovelace, K. Kuper, M. Boyle, B. Szilagyi, and L. E. Kidder, Class. Quantum Grav. **32**, 105009 (2015) [arXiv:1412.1803 [gr-qc]] [Search INSPIRE].
[13] S. A. Teukolsky, Astrophys. J. **185**, 635 (1973).
[14] J. M. Bardeen, W. H. Press, and S. A. Teukolsky, Astrophys. J. **178**, 347 (1972).
[15] H. Yang, D. A. Nichols, F. Zhang, A. Zimmerman, Z. Zhang, and Y. Chen, Phys. Rev. D **86**, 104006 (2012) [arXiv:1207.4253 [gr-qc]] [Search INSPIRE].
[16] B. F. Schutz and C. M. Will, Astrophys. J. **291**, L33 (1985).
[17] M. Sasaki and T. Nakamura, Phys. Lett. A **89**, 68 (1982).
[18] M. Sasaki and T. Nakamura, Prog. Theor. Phys. **67**, 1788 (1982).
[19] T. Nakamura and M. Sasaki, Phys. Lett. A **89**, 185 (1982).
[20] S. L. Detweiler, Proc. R. Soc. Lond. A **352**, 381 (1977).
[21] F. Pretorius, Phys. Rev. Lett. **95**, 121101 (2005) [arXiv:gr-qc/0507014] [Search INSPIRE].
[22] M. Campanelli, C. O. Lousto, P. Marronetti, and Y. Zlochower, Phys. Rev. Lett. **96**, 111101 (2006) [arXiv:gr-qc/0511048] [Search INSPIRE].
[23] J. G. Baker, J. Centrella, D. I. Choi, M. Koppitz, and J. van Meter, Phys. Rev. Lett. **96**, 111102 (2006) [arXiv:gr-qc/0511103] [Search INSPIRE].
[24] L. London, D. Shoemaker, and J. Healy, Phys. Rev. D **90**, 124032 (2014) [arXiv:1404.3197 [gr-qc]] [Search INSPIRE].
[25] http://www.black-holes.org/waveforms/, date last accessed February 23, 2016.

[26] E. Berti, V. Cardoso, and C. M. Will, Phys. Rev. D **73**, 064030 (2006) [arXiv:gr-qc/0512160] [Search INSPIRE].
[27] http://www.phy.olemiss.edu/∼berti/ringdown/, date last accessed February 23, 2016.
[28] H. Nakano, T. Tanaka, and T. Nakamura, Phys. Rev. D **92**, 064003 (2015) [arXiv:1506.00560 [astro-ph.HE]] [Search INSPIRE].
[29] T. Kinugawa, K. Inayoshi, K. Hotokezaka, D. Nakauchi, and T. Nakamura, Mon. Not. R. Astron. Soc. **442**, 2963 (2014) [arXiv:1402.6672 [astro-ph.HE]] [Search INSPIRE].
[30] T. Kinugawa, A. Miyamoto, N. Kanda, and T. Nakamura, Mon. Not. R. Astron. Soc. **456**, 1093 (2016) [arXiv:1505.06962 [astro-ph.SR]] [Search INSPIRE].
[31] S. Hod, Phys. Rev. D **78**, 084035 (2008) [arXiv:0811.3806 [gr-qc]] [Search INSPIRE].
[32] G. B. Cook and M. Zalutskiy, Phys. Rev. D **90**, 124021 (2014) [arXiv:1410.7698 [gr-qc]] [Search INSPIRE].
[33] M. Sasaki and T. Nakamura, Gen. Relat. Gravit. **22**, 1351 (1990).